TITLE:

DIFFERENTIAL EFFECTS OF REACTIVE OXYGEN SPECIES ON AUTOPHAGY IN ARABIDOPSIS

RUNNING TITLE:

Redox regulation of autophagy

AUTHORS:

Alejandro Enet [1†], Germán Robert [1,2,3 † *], Laura Saavedra [1], Ramiro Lascano [1,2 *]

[†] Both authors contributed equally

*** Corresponding authors:**

robert.german@inta.gob.ar; ramiro.lascano@unc.edu.ar

AFFILIATIONS

[1] Plant Stress Biology Group, Unidad de Doble Dependencia INTA-CONICET (UDEA), Av. 11 de Septiembre, Córdoba 4755-X5020ICA, Argentina.

[2] Cátedra de Fisiología Vegetal, Facultad de Ciencias Exactas Físicas y Naturales, Universidad Nacional de Córdoba, Av. Velez Sarsfield 299, Córdoba, Argentina;

[3] Instituto Nacional de Tecnología Agropecuaria (INTA), Instituto de Fisiología y Recursos Genéticos Vegetales (IFRGV), Av. 11 de Septiembre, Córdoba 4755-X5020ICA, Argentina.

Alejandro Enet: ale.403@hotmail.com

Germán Robert: robert.german@inta.gob.ar

Laura Saavedra: saavedra.laura@inta.gob.ar

Ramiro Lascano: ramiro.lascano@unc.edu.ar

KEYWORDS

Autophagy, stress, reactive oxygen species, singlet oxygen, superoxide radical, hydrogen peroxide, redox state, Arabidopsis thaliana.

HIGHLIGHT

This research shows the differential effects of reactive oxygen species on autophagic flux, highlighting their impact on the cytoplasmic redox state.

ABSTRACT

Autophagy plays a key role in the responses to different stress condition in plants. Reactive oxygen species (ROS) are common modulators of stress responses, having both toxic and signaling functions. In this context, the relationship between ROS and autophagy regulation remains unclear, and in some aspects, contradictory. In this study, we employed pharmacological and genetic approaches to investigate the effects of different ROS on the cytoplastic redox state and autophagic flux in *Arabidopsis thaliana*. Ours results demonstrated that oxidative treatments with H_2O_2 and MV, which drastically increased the oxidized state of the cytoplasm, reduced the autophagic flux. Conversely, singlet oxygen, which did not have significant effects on the cytoplasmic redox state, increased the autophagic flux. Additionally, our findings indicated that after H_2O_2 and high light treatments and during the recovery period, the cytoplasm returned to its reduced state, while autophagy was markedly induced. In summary, our study unveils the differential effects of ROS on the autophagic flux, establishing a correlation with the redox state of the cytoplasm. Moreover, it emphasizes the dynamic nature of autophagy in response to oxidative stress and the subsequent recovery period.

KEYWORDS

Autophagy, stress, reactive oxygen species, singlet oxygen, superoxide radical, hydrogen peroxide, redox state, Arabidopsis thaliana.

ABBREVIATIONS

ATG: autophagy genes
Conc A: Concanamicina A
GFP: green fluorescent protein
GSH: reduced glutathione
GSSG: oxidized glutathione
MV: methyl viologen
roGFP: redox-sensitive green fluorescent proteins
ROS: reactive oxygen species

97 **INTRODUCTION**

98 Plants as sessile organisms are constantly exposed to different biotic and abiotic stress
99 conditions, so they have evolved integrated defense and acclimation mechanisms to cope with
100 adverse conditions (Fichman and Mittler, 2020; Peláez-vico *et al.*, 2022). A common effect
101 induced in plants by different stress conditions is the increase in the generation of reactive
102 oxygen species (ROS), such as superoxide (O_2^-), hydrogen peroxide (H_2O_2), singlet oxygen ($^1O_2$),
103 and the hydroxyl radical (-OH), at different subcellular compartments, such as chloroplasts,
104 mitochondria, peroxisomes, cytosol and the apoplast (Apel and Hirt, 2004; Foyer and Noctor,
105 2009, 2011*a*). ROS are potent oxidants, that depending on their intensity, duration, and location
106 site of production within the cell can modify different biomolecules, affecting the redox state in
107 different subcellular compartments, provoking oxidative stress, inducing senescence symptoms
108 and cell death. Furthermore, due to their high reactivity and toxicity, the maintenance of tightly
109 regulated ROS levels becomes crucial for plant acclimation, adaptation, and survival, facilitated
110 by the activity of a sophisticated plant antioxidative system (Apel and Hirt, 2004; Foyer and
111 Noctor, 2009, 2011*b*; Trippi *et al.*, 2009). In this way, controlling the different types of ROS
112 produced, along with their intensity, duration, and site of production, has diverse implications
113 in redox signaling, influencing processes such as growth, development, and responses to
114 changing environmental conditions (Melchiorre *et al.*, 2009; Miller *et al.*, 2009; Robert *et al.*,
115 2009, 2018; Muñoz *et al.*, 2012; Fernandez-göbel *et al.*, 2019; Fichman and Mittler, 2020;
116 Zandalinas *et al.*, 2020; Peláez-vico *et al.*, 2022). Consequently, ROS are recognized as critical
117 signaling molecules, and the cellular redox state is considered an intensive property of the living
118 system that integrates information from metabolic, energetic and environmental cues
119 controlling growth, development and acclimation responses, as well as cell suicide events
120 (Breusegem and Dat, 2006; Trippi *et al.*, 2009; Fichman and Mittler, 2020; Peláez-vico *et al.*,
121 2022).

122 In plants, chloroplast, mitochondria and peroxisome, which are redox active organelles
123 where carbon and energetic metabolisms take place, are major sources of ROS production (Apel
124 and Hirt, 2004). In chloroplasts, the photosynthetic process involves physical, biophysical, and
125 biochemical redox reactions with different reaction rates. In consequence, oxygen became a
126 potent univalent electron or energy acceptor from highly activated intermediates under
127 conditions of excess excitation energy (EEE) (Karpinski *et al.*, 1999; Foyer and Hanke, 2022). ROS
128 produced in the chloroplasts are particularly important in the retrograde signaling of EEE
129 conditions, affecting nuclear gene expression, acclimation responses as well as programmed cell
130 death (Karpinski *et al.*, 1999; Breusegem *et al.*, 2001; Breusegem and Dat, 2006; Bechtold *et al.*,
131 2008; Fichman and Mittler, 2020; Foyer and Hanke, 2022).

132 Likewise, several stress conditions in plants have been also shown to be capable of
133 triggering or increasing autophagy (Signorelli *et al.*, 2019; Wang *et al.*, 2021). Autophagy is an
134 ancient and conserved process in eukaryotes by which different cellular components are
135 delivered to vacuole/lysosome to be degraded, and is essential for plant energetic metabolisms,
136 growth, development and response to different stress conditions (Su *et al.*, 2020; Wang *et al.*,
137 2021). Different types of autophagy have been identified in plants (Yoshimoto, 2012).
138 Macroautophagy (hereafter termed autophagy) is the type of autophagy most thoroughly
139 studied in all organisms. The autophagic process is initiated, and mainly modulated in the
140 cytosol, by the formation of a double membrane cup, the phagophore, that expands to engulf
141 macromolecules and cellular components to finally form a double-membrane vesicle called

142 autophagosomes. The autophagosomes are then transported and fused with the vacuole,
143 facilitating the delivery of their cargo for subsequent degradation (Yoshimoto, 2012; Yoshimoto
144 and Ohsumi, 2018). The several steps of the autophagic process are coordinated by ATG
145 (AuTophaGy) proteins as well as by some components of the endosome pathway, as recently
146 reported (Zhuang *et al.*, 2015; Yoshimoto and Ohsumi, 2018; Robert *et al.*, 2021). While early
147 evidence pointed to a strong transcriptionally regulation of autophagy in response to nutritional
148 starvation conditions and foliar senescence (Yoshimoto *et al.*, 2004; Breeze *et al.*, 2011), recent
149 studies have shed light on the widespread modulation of autophagy initiation and progression
150 by post-translational modifications of core autophagy proteins. These modifications primarily
151 occur at the cytoplasmic level in response to environmental cues (Feng *et al.*, 2015; Yang *et al.*,
152 2019; Qi *et al.*, 2021; Agbemafle *et al.*, 2023).

153 It has been suggested a positive correlation between ROS generation and the autophagic
154 process, where ROS can serve as both sources of damage and signals (Xiong *et al.*, 2007*a*,*b*;
155 Signorelli *et al.*, 2019). Autophagy promotes the degradation of ROS-overproducing damaged
156 organelles including chloroplasts, mitochondria, and peroxisomes, thus fulfilling antioxidant
157 roles (Xiong *et al.*, 2007*b*; Shibata *et al.*, 2013; Nakamura *et al.*, 2018; Oikawa *et al.*, 2022).
158 Supporting this notion, observations in different autophagy-mutant plants demonstrate the
159 accumulation of oxidized and ubiquitinated proteins (Xiong *et al.*, 2007*a*; Munch *et al.*, 2014),
160 high levels of H_2O_2 (Yoshimoto *et al.*, 2009), increased amounts of total glutathione (Masclaux-
161 Daubresse *et al.*, 2014), accelerated senescence (Doelling *et al.*, 2002; Hanaoka *et al.*, 2002;
162 Yoshimoto *et al.*, 2004), and hypersensitivity to different stress conditions including oxidative
163 stresses (Xiong *et al.*, 2007*b*; Liu *et al.*, 2009; Zhou *et al.*, 2013), indicating a significant redox
164 imbalance. On the other hand, oxidative treatments with H_2O_2 and methyl viologen (MV) have
165 been shown to induce autophagy (Xiong *et al.*, 2007*b*; Pérez-Pérez *et al.*, 2012*b*). Likewise,
166 autophagosome formation triggered by nutritional starvation and saline stress in Arabidopsis
167 roots depends on the NADPH-oxidase complex, a major source of ROS in the apoplast, which is
168 essential for local and systemic redox signal transduction (Liu *et al.*, 2009). However, the
169 induction of autophagy under osmotic stress was shown to be NADPH oxidase-independent,
170 suggesting that different signaling pathways regulate autophagy induction, and in certain
171 scenarios are dependent on ROS signaling (Liu *et al.*, 2009). More recently, it has been
172 hypothesized that H_2O_2 accumulation and membrane damage may mediate chlorophagy
173 induced by UV and high light treatments in Arabidopsis leaves (Izumi *et al.*, 2017; Woodson,
174 2019). Consequently, it is plausible that autophagy induction occurs as a response to the
175 accumulation of cellular components that have been damaged. Notably, recent studies
176 conducted in yeast, animals and Chlamydomonas have revealed that certain proteins involved
177 in the autophagic process could be inhibited by ROS in *in vitro* experiments or artificial oxidative
178 stress *in vivo*, indicating that ROS may inhibit the function of some autophagy-related proteins
179 (Pérez-Pérez *et al.*, 2014, 2016; Frudd *et al.*, 2018). These findings raise apparently opposite
180 evidence regarding the redox regulation of autophagy. Hence, the picture about the relationship
181 among different ROS, subcellular redox changes, and autophagy regulation in plants is still
182 unclear. Under this scenario, our study aimed to address the effects of different ROS on
183 autophagy in plants.

184 Herein, we provide evidence that oxidative treatments with H_2O_2 and MV, which
185 drastically increased the oxidized state of the cytoplasm, led to a reduction in the autophagic
186 flux in Arabidopsis seedlings. Likewise, after the oxidative treatments and during the subsequent

recovery period, the cytoplasm returned to its reduced state while autophagy was markedly induced. On the other hand, pharmacological and genetic approaches widely used to enhance the generation of $^1O_2$ resulted in an increased autophagic flux in Arabidopsis seedlings, with no significant effects observed on the cytoplasmic redox state. In summary, our findings unveil the distinct effects of ROS on autophagic flux, highlighting a strong correlation between autophagy and the physicochemical properties of the cytoplasm, with autophagy inhibition occurring under conditions where the redox state of the cytoplasm is highly oxidized.

MATERIALS AND METODS

Plant materials and growth conditions.

Arabidopsis thaliana ecotype Columbia (Col-0) was used in this study. 35S:GFP-ATG8a transgenic seeds (CS39996) (Thompson et al., 2005) were obtained from the Arabidopsis Biological Resource Center. The cytosol-targeted fluorescent redox sensors GFP2-Orp1 or GRX-roGFP2 were provided by Dr. Markus Schwarzländer. Fluorescent (*flu*) and ferrochelatase 2 (*fc2*) mutants were provided by Dr. Jesse Woodson. We introgressed the GFP-ATG8a, GFP2-Orp1 and GRX-roGFP2 transgenes into the *flu* and *fc2* mutant lines by genetic crosses. Homozygous offspring were then selected from the F3 backcross generations.

Seeds were surface-sterilized and sown on culture plates containing nutrient-rich Murashige and Skoog (MS) solid medium lacking sucrose and containing 1 % agar. After sowing, plates were kept in darkness at 4°C for 2 to 3 days, and then transferred to a growth chamber under a 16 h light/8 h dark photoperiod. Photosynthetic photon flux density was 110 µmol m^{-2} sec^{-1}. Average temperature was 22°C. Plants were grown for 7 days under these conditions and then passed to MS liquid medium to carry out the different treatments. For salt and osmotic stresses, NaCl (50 mM) and mannitol (100 mM) were used, respectively. Oxidative treatments were performed by the supplementation of the MS liquid medium with 1 µM methyl viologen (MV), 10 mM H_2O_2, 20 µM 3-(3,4-dichlorophenyl)-1,1-dimethylurea (DCMU), 20 µM methylene blue (MB). To scavenge superoxide and peroxide, 10 mM tiron and 10 mM benzoic acid (BA) were co-administrated, respectively. 10 mM dithiothreitol (DTT) was used as a reducing agent for protein disulfide bonds.

Confocal fluorescence microscopy and image analysis.

Confocal microscopy was performed on an Inverted microscope Nikon Eclipse CZ1. 35S:GFP-ATG8a expressing plants were observed with a 488-nm argon laser (BP 495–530 nm). To analyze autophagic bodies accumulation, 1 µM Concanamycin A was added to the different treatments. The number of autophagic bodies in epidermal cells was quantified after 16 h of treatments using ImageJ by counting their numbers in the central vacuole of multiple cells in sections of 50000 μm^2. A macro for automating autophagosome counting was developed in ImageJ. Briefly, the input images were converted into an 8-bit format, followed by background subtraction using a rolling ball algorithm with a 50-pixel radius. Subsequently, particle analysis was performed on the binary image, considering particle size, circularity, and displaying the resulting masks.

Cytosol-targeted fluorescent redox sensors GFP2-Orp1 or GRX-roGFP2 were excited at 488 nm and 405 nm and fluorescent emissions were collected at 505-535 nm. All imaging parameters were kept constant throughout all measurements. Subsequently, a single ratiometric image was generated using the ImageJ software, where the value of each pixel is the product of the ratio between the intensity at 405 nm with respect to that obtained at 488 nm according to (Schwarzlander *et al.*, 2008). Quantitative measurements were calculated as the ratio of the mean intensity from each channel. The dynamic range of these reporter lines was established

234 using 10 mM DTT and a curve of increasing concentrations of H_2O_2. For pseudocolor display, the
235 ratio was coded on a spectral color scale ranging from blue (fully reduced) to red (fully oxidized).
236
237 **Immunoblot analyses.**
238 For GFP-ATG8 cleavage assay, seven-day old 35S:GFP-ATG8a transgenic plants were transferred
239 to MS liquid medium to carry out the different treatments for 6 h. Then, total proteins were
240 extracted. The extracts were centrifuged at 10 000 g for 10 min, and equal amounts of proteins
241 from the supernatants were subjected to SDS-PAGE and immunoblotted with anti-GFP
242 antibodies (Roche). Comparisons of absolute integrated density values for each line (GFP-ATG8
243 and free GFP) were made. Corresponding background values were subtracted from integrated
244 density values, then integrated density values for bands corresponding to free GFP were
245 expressed as relative values of GFP-ATG8 present in the same sample, and relativized to a
246 control condition.
247
248 **Physiological parameters.**
249 Seven-day old Arabidopsis seedlings were exposed to the different treatments for 8 h and then
250 the production of H_2O_2 and O_2^-, quantum efficiency of PSII photochemistry (ΦPSII), as well as the
251 content of chlorophyll, soluble sugars and malondialdehyde (MDA) were analyzed. To assess
252 H_2O_2 and O_2^- accumulation, leaves were stained with DAB and NBT, respectively. The staining
253 was quantified by measuring the intensity per area using ImageJ. Quantum efficiency of PSII
254 photochemistry (ΦPSII) was measured from the upper surface using a pulse amplitude
255 modulated fluorometer (FMS2, Hansatech Instruments, Pentney King's Lynn, UK).
256 Measurements were performed 6 h after the growth chamber lights were turned on. For
257 chlorophyll, soluble sugars, and MDA analysis an alcoholic extract (1:2 w/v) was obtained from
258 the samples. After centrifugation for 15 minutes at 12,000 *g*, the supernatant was diluted in
259 ethanol, and the absorbance was measured at 654 nm using a spectrophotometer. Total
260 chlorophylls were calculated following the method reported by (Wintermans M. and De Mots
261 A., 1965). For soluble sugars determination, an aliquot of the sample was dried, and
262 resuspended in a same volume of water. Then, the concentration of sugars was measured with
263 anthrone (Fales, 1951) evaluating the absorbance at 620 nm using a glucose standard curve. For
264 MDA determination, a volume of the supernatant was mixed with a same volume of a mixture
265 of 0,5 % TBA and 20 % TCA, and incubated 20 minutes at 90 °C. The mixture was centrifuged at
266 12,000 *g* for 5 minutes, and the absorbance was measured at 532 and 600 nm (Heath and Packer,
267 1968).
268
269 **RNA extraction and RT-qPCR**
270 Samples were homogenized in a cold mortar with TRIzol Reagent, mixed for 1 min and incubated
271 at room temperature for 5 min. Then, 0.2 ml chloroform per ml of TRIzol Reagent was added and
272 incubated at room temperature for 3 min. After incubation, the samples were centrifuged at 12
273 000 *g* at 4 °C for 15 min and the aqueous phases were transferred to clean tubes. RNA was
274 precipitated by adding 1 vol of isopropanol, incubated at room temperature for 10 min and
275 centrifuged at 12 000 *g* at 4 °C for 15 min. The precipitate was washed with 70 % ethanol and
276 the samples were centrifuged again at 12 000 *g* at 4 °C for 15 min. The precipitates were dried
277 and resuspended in diethyl pyrocarbonate-treated water and its concentration was quantified
278 using a NanoDrop 3300 spectrometer (Thermo Scientific). Purified RNA was treated with DNase
279 I (Invitrogen) to remove genomic DNA, according to the manufacturer's instructions. DNA-free
280 RNA (1 to 2.5 µg) was used with oligo(dT) for first strand cDNA synthesis using the Moloney
281 murine leukemia virus reverse transcriptase (M-MLV RT, Promega) according to the
282 manufacturer's instructions. For each primer pair, the presence of a unique product of the

283 expected size was checked on ethidium bromide-stained agarose gels after PCR reactions.
284 Absence of contaminant genomic DNA was confirmed in reactions with DNase-treated RNA as
285 template. The qPCR reaction was performed using iQ Universal SYBR Green Supermix (Bio-Rad).
286 Amplification of actin with the forward primer 5'-TTCAGATGCCCAGAAGTCTTG-3' and the
287 reverse primer 5-GCGATACCTGAGAACATAGTGG-3 was used to normalize the amount of
288 template cDNA. The specific primers pair employed for the detection of *Atg6* was forward primer
289 5'-AAAACTGGGAGAGCGATGAG-3' and reverse primer 5'-GATAGATGAGCCCTGCGTAG-3', for
290 *Atg4a* was 5'-CCTTTGGAATCACTCGACCCATCT-3' and 5'-ATCCGCAAACCCGTAGTTGCTT-3', for
291 *Atg7* was 5'-GCGGCTTTAGGTTTTGACAG-3' and 5'-GTTGGTCTAGAGTTCGATCAGTC -3', and for
292 *Atg5* was 5'-TCCTGTTCGGTTGTATGTTCG-3' and 5'-CGCTCTGTCTCCCATAAACTC-3'. qPCR was
293 performed in thermocycler iQ5 (Bio-Rad) at 59 °C with iQ SYBR Green Supermix (Bio-Rad),
294 according to the manufacturer's instruction. Relative transcript abundance was calculated (Livak
295 and Schmittgen, 2001).
296
297 **Microarray analysis.**
298 Publicly available microarray data were utilized to compare the expression of *Atg* genes under
299 various conditions, including nitrogen deficiency (Rubin *et al.*, 2009), treatment with 10 mM
300 H_2O_2 for 24 h (Willems *et al.*, 2016), treatment with 10 µM MV for 2 h (Scarpeci *et al.*, 2008),
301 and the examination of *flu* mutant plants subjected to an 8-hour cycle of darkness followed by
302 2 h of light (Op Den Camp *et al.*, 2003). Expression values were normalized to the corresponding
303 control conditions employed in each study and were expressed as $\log_2$ values.
304
305 **Statistical analyses.**
306 Data were analysed by analysis of variance (ANOVA) followed by the Di Rienzo–Guzman–
307 Casanoves (DGC) test model, a cluster-based method for identifying groups of non-
308 homogeneous means, using InfoStat software (Di Rienzo *et al.*, 2002).
309
310 **RESULTS**
311 **H_2O_2 and methyl viologen treatments oxidized the cytoplasmic redox state and inhibited**
312 **autophagy in Arabidopsis.**
313 Initially, to gain insights into the interplay between ROS, redox state changes and
314 autophagy, *Arabidopsis thaliana* seedlings were subjected to well-established autophagy-
315 inducing conditions, namely nutritional starvation and different abiotic stress treatments (Wang
316 *et al.*, 2021), and both autophagy and the cytoplasmic redox state were analyzed (Fig. 1). To
317 monitor autophagy, 35S:GFP-ATG8a (GFP-ATG8) transgenic plants were grown 7 days in MS solid
318 medium, and then transferred to the different treatments in MS liquid medium supplemented
319 with 1 µM Concanamycin A (Conc A) for a 16 hour-period. Conc A is a V-ATPase inhibitor widely
320 used to prevent vacuole acidification, thereby effectively inhibiting the lytic activity of vacuoles,
321 thus allowing the detection of autophagic bodies accumulation into the vacuoles through
322 confocal microscopy (Fig. 1A and B). Analysis of autophagic flux using Conc A better defines
323 autophagic activity since the increase of autophagosome number in the cytoplasm does not
324 necessarily corresponds to an enhanced autophagic activity (Robert *et al.*, 2021). When
325 subjected to carbon and nitrogen starvation treatments, epidermal cells showed a high
326 accumulation of autophagic bodies in the vacuole compared to control conditions, indicating an
327 activated autophagic flux (Fig. 1A and B). Similarly, saline and osmotic stress treatments resulted
328 in comparable outcomes, with a significant increase in autophagic bodies accumulating within
329 the vacuoles (Fig. 1A and B). Besides, to evaluate the cytoplasmic redox state *in vivo*, 7 days old
330 transgenic plants expressing the cytosol-targeted fluorescent redox sensors GFP2-Orp1 or GRX-

331 roGFP2 were subjected to the different treatments (Fig. 1). These transgenic plants express
332 redox-sensitive green fluorescent proteins (roGFPs) genetically fused to different redox-active
333 proteins sensing H_2O_2 production and GSH:GSSG, respectively (Schwarzländer *et al.*, 2009, 2015;
334 Aller *et al.*, 2013; Nietzel *et al.*, 2019). The relative intensity of the two fluorescence excitation
335 maxima depends on the redox state of the modified GFP, enabling ratiometric measurements,
336 independent of the probe concentration (Schwarzländer *et al.*, 2016). The dynamic range of
337 these reporter lines was previously monitored using DTT and H_2O_2 (Fig. S1). Notably, in
338 epidermal cells of seedlings expressing either GFP2-Orp1 or GRX-roGFP2, no changes in the
339 cytoplasmic redox state were detected after 16 h of nutritional starvation, neither under saline
340 or osmotic stress treatments compared to control conditions (Fig. 1A and C). These findings align
341 with earlier assessments of the redox state in cells of GRX-roGFP2 and roGFP2-ORP1 plants
342 under different stress conditions (Schwarzländer *et al.*, 2009).
343 To further investigate the interplay between ROS, redox state changes and autophagy,
344 oxidative stress treatments using H_2O_2 and methyl viologen (MV) were conducted. We evaluated
345 different concentrations of H_2O_2 and observed a dose-dependent response for both the
346 oxidation of the cytoplasmic redox state and autophagy inhibition (Fig. S1). A similar approach
347 was taken with MV, an herbicide widely used for the induction of photooxidative stress as it
348 takes electrons from photosystem I, generating O_2^- and H_2O_2 inside chloroplasts in the presence
349 of light (Mehler, 1951; Farrington *et al.*, 1973; Lascano *et al.*, 2012; Nazish *et al.*, 2022). Based
350 on these results and with the intention of employing moderate oxidative stress conditions that
351 do not induce cell death, we used 10 mM H_2O_2 and 1 µM MV for subsequent experiments.
352 Although oxidative treatments have been reported as autophagy-inducing conditions in
353 Arabidopsis and Chlamydomonas (Xiong *et al.*, 2007*b*; Pérez-Pérez *et al.*, 2012*b*), no significant
354 differences were observed in the accumulation of autophagic bodies in the epidermal cells of
355 seedlings treated with MV or H_2O_2 compared to the control condition (Fig. 1A and B). In contrast
356 to observations under autophagy-inducing conditions such as nutritional starvation, saline, or
357 osmotic stresses, these oxidative treatments significantly oxidized the cytoplasmic redox state,
358 as indicated by the reduced GSSG:GSH ratio in the cytoplasm (GRX-roGFP2) and increased the
359 accumulation of H_2O_2, as revealed by analyzing roGFP2-ORP1 plants and DAB staining (Fig. 1A
360 and C; Fig. 2; Fig. S1; Fig. S2).
361 To further characterize the effects of oxidative stress on autophagy, treatments with MV
362 and H_2O_2 were performed on 35S:GFP-ATG8a plants under autophagic inducing conditions,
363 specifically nitrogen and carbon starvation (Fig. 2). Interestingly, treatments with MV and H_2O_2
364 reduced the accumulation of autophagic bodies after 16 h of starvation conditions (Fig. 2A and
365 B). Furthermore, the inhibitory effects of the oxidative treatments on the autophagic flux were
366 also confirmed by analyzing the degradation of the GFP-ATG8a fusion protein by western blot
367 (Fig. 2D). The evaluation of autophagic flux through the analysis of the degradation of the GFP-
368 ATG8 fusion protein by immunoblotting allowed us to examine the effects of oxidative stress on
369 autophagy in shorter time periods (6 h, Fig. 2D).. Next, tiron and benzoic acid were co-
370 administered with the MV treatment to scavenge superoxide and hydrogen peroxide
371 (Navabpour *et al.*, 2003; Mansouri *et al.*, 2005; Velika and Kron, 2012; Liubimovskii *et al.*, 2021).
372 The effects of MV on autophagic flux, H_2O_2 accumulation, and cytoplasmic redox state oxidation
373 were blocked in the presence of ROS scavengers (Fig. 2, Fig. S2). Similarly, photooxidative
374 treatments induced by high light treatments showed an inhibitory effect on the autophagy flux,
375 which was reversed in the presence of the superoxide radical scavenger, tiron (Fig. 2D).
376 Moreover, both tiron and benzoic acid prevented photosynthetic damage caused by MV
377 treatments, as measured by the quantum yield of photosystem II (ΦPSII), and prevented the
378 decrease in soluble sugar levels (Fig. S2). Furthermore, the inhibitory effects of MV on

379 autophagic flux and the oxidation of the GSH:GSSG sensor probe (GRX-roGFP2) were reversed
380 when 10 mM dithiothreitol (DTT), a reducing agent for protein disulfide bonds, was added (Fig.
381 S2). These results emphasize that the effects of MV in plants are associated with its capacity to
382 induce ROS generation, contributing to a more oxidized cellular redox state and oxidative
383 damage (Lascano *et al.*, 2012). Notably, the restoration of autophagic flux in MV-treated plants
384 by tiron, benzoic acid, and DTT suggests that H_2O_2 may inhibit autophagy, potentially by oxidizing
385 disulfide bonds in crucial ATG proteins (Fig. S3 and S4) as demonstrated in recent studies in
386 yeast, Chlamydomonas, and animals (Pérez-Pérez *et al.*, 2014, 2016; Frudd *et al.*, 2018; Zheng
387 *et al.*, 2020). In this regard, the inhibitory effect of H_2O_2 treatments on autophagy was also
388 observed in plants exposed to carbon or nitrogen starvation (Fig. 2A, B and D; Fig. S1).
389
390 **Autophagy is induced in the recovery phase after oxidative stress in Arabidopsis.**
391 Previous reports indicated that autophagy is involved in degrading oxidized proteins and
392 organelles in response to oxidative stress (Xiong *et al.*, 2007*b*; Shibata *et al.*, 2013; Izumi *et al.*,
393 2017; Oikawa *et al.*, 2022). However, our experimental results demonstrate that oxidative stress
394 treatments inhibit autophagy, as illustrated in Figure 2. In light of these findings, we aimed to
395 investigate autophagic activity following oxidative stress treatments by assessing the autophagic
396 flux in Arabidopsis plants during the recovery phase. With this purpose, 7-day-old Arabidopsis
397 seedlings were subjected to a brief exposure of 10 mM H_2O_2 or high light intensity (≈1000
398 µmoles m^{-2} s^{-1}) for 4 hours, followed by transfer to H_2O_2-free MS liquid medium under control
399 conditions (≈100 µmoles m^{-2} s^{-1}) for a 20-hour recovery period. Additionally, a set of plants were
400 incubated in 10 mM H_2O_2 or to control conditions (H_2O_2-free MS liquid medium) for 24 h. This
401 experimental design aimed to elucidate the dynamic changes in autophagy following oxidative
402 stress and determine whether autophagic activity is modulated during the recovery phase. The
403 results showed that autophagic flux was inhibited in plants incubated 24 h with H_2O_2 compared
404 to control conditions (Fig. 3A, B and D). However, autophagic flux was not only recovered but
405 also induced during the recovery period after the stress treatments surpassing the levels
406 observed in plants subjected to control conditions (Fig. 3A, B and D). Likewise, after the 20-hour
407 recovery period, the redox biosensors returned to their reduced state, indicating both a
408 successful cytoplasmic redox recovery, and a well-defined correlation between reduced
409 cytoplasmic redox state and autophagic flux (Fig. 3A and C).
410
411 **Singlet oxygen induced autophagic flux but did not affect the cytoplasmic redox state.**
412 Singlet oxygen ($^1O_2$) is mainly produced in the chloroplast, and its targets are
413 predominantly confined inside this organelle due to the specific physicochemical characteristic
414 of this ROS (Dmitrieva *et al.*, 2020). To investigate the effects of $^1O_2$ on the autophagic activity,
415 GFP-ATG8a seedlings were treated with 3-(3,4-dichlorophenyl)-1,1-dimethylurea (DCMU) (Fig.
416 4), an herbicide that specifically induces $^1O_2$ generation by blocking plastoquinone reduction.
417 This process promotes $^1O_2$ generation without affecting superoxide anion and hydroxyl radicals
418 at PSII (Fufezan *et al.*, 2002; Flors *et al.*, 2006; Dmitrieva *et al.*, 2020). The analysis of autophagic
419 body accumulation and cytoplasmic redox state was conducted after a 16-hour treatment (Fig.
420 4A-C). Additionally, treatments with methylene blue (MB), a type-II photosensitizer able to
421 generate $^1O_2$ in leaves under visible light (Shao *et al.*, 2007, 2013), with minor effects on
422 photosynthesis (Fig. 4E), were also performed. Treatments with these chemicals increased the
423 accumulation of autophagic bodies but did not show statistically significant effects on the redox
424 state of the cytoplasm and H_2O_2 production in Arabidopsis cells compared to control treatment
425 (Fig. 4A and B). The autophagic flux-inducing effect of DCMU and MB was also evidenced after

426 6 hours of treatments through the analysis of GFP-ATG8 degradation by immunoblotting (Fig.
427 4D).
428 To further investigate the effects of $^1O_2$ on the autophagic process and the cytoplasmic
429 redox state, autophagy reporter- and redox sensor-transgenic plants were crossed with widely
430 used endogenously chloroplast $^1O_2$-hyperproducing *Arabidopsis* mutant plants: fluorescent (*flu*)
431 and two different lines of ferrochelatase 2 (*fc2*): *fc2.1* which presents reduced expression levels
432 of *Fc2*, and the null mutant *fc2.2*. These mutant plants accumulate different photosensitizing
433 intermediates of chlorophyll biosynthesis in the dark, which, upon light exposure lead to an
434 exacerbated production of $^1O_2$ (Op Den Camp *et al.*, 2003). The *flu* mutant plants accumulate
435 protochlorophyllide (Meskauskiene *et al.*, 2001), while mutations in plastid ferrochelatase 2 lead
436 to the accumulation of protoporphyrin IX (Scharfenberg *et al.*, 2015). Initially, wild type, *flu* and
437 *fc2* mutant plants were grown 7 days under continuous light conditions (control conditions), and
438 several growth and physiological parameters were evaluated (Fig. S5). Interestingly, the *fc2*
439 mutants showed arrested root growth, reduced chlorophyll levels, increased levels of
440 malondialdehyde (MDA) an intermediary metabolite of lipid peroxidation used as oxidative
441 stress marker (Robert *et al.*, 2014), and reduced levels of soluble sugars compared to wild type,
442 while no significant differences were observed between wild type and *flu* mutant (Fig. S5).
443 Likewise, the cytoplasmic redox state in *fc2* plants was significantly more oxidized than that in
444 the wild type and *flu* backgrounds (Fig. S5, Fig. 5). Furthermore, and consistent with a previous
445 study (Lemke *et al.*, 2021), the autophagic flux was induced in *fc2* mutants plants compared to
446 wild type and *flu* mutant under continuous light conditions (Fig. S5). Hence, considering the
447 altered phenotypes observed in *fc2* mutants even under control conditions, we used the *flu*
448 mutants for subsequent analysis.
449 *flu*/GFP-ATG8a plants were grown under continuous light conditions for 7 days,
450 transferred to darkness for 8 h, and then re-exposed to light in the presence of Conc A for
451 another 8 h. After the light/dark/light cycling conditions, a significantly increased autophagic
452 flux was observed in *flu*/GFP-ATG8a compared to Col-0/GFP-ATG8 plants. However, no
453 statistically significant differences were observed among these genotypes under continuous
454 light conditions (Fig. 5A, B and D). Besides, the accumulation of H_2O_2 was monitored under
455 control conditions as well as after a period of darkness by analyzing the fluorescent redox sensor
456 roGFP2-ORP1 expressed in the wild type and *flu* backgrounds. Although a slight tendency
457 towards a more oxidized state was observed in the cytoplasm of *flu* mutant plants once re-
458 exposed to light, the differences were not statistically significant (Fig. 5C). Thus, in contrast to
459 H_2O_2 and MV treatments, $^1O_2$ increased the autophagic flux and did not oxidize the cytoplasmic
460 redox state, indicating differential effects on the autophagic activity depending on the ROS
461 nature and their effects on the cytoplasmic redox state. Moreover, the transcript levels of *Atg4*,
462 *Atg5*, *Atg6* and *Atg7* were analyzed by RTq-PCR in *flu* mutant after 8 h of light re-exposure. No
463 statistically significant differences were observed in the expression level of the analyzed genes
464 between wild type and *flu* mutant neither under control conditions nor after cycling conditions
465 (Fig. S6).
466
467 **DISCUSSION**
468 Plants, as aerobic and sessile organisms, respond to environmental stresses by
469 increasing the production of reactive oxygen species (ROS), which, due to their high reactivity,
470 fulfill dual roles by acting both as agents of damage and as signaling molecules. Consequently,
471 ROS are universally implicated in plant stress symptomatology, and also play a pivotal role in
472 modulating plant growth, development, and cell death (Apel and Hirt, 2004; Trippi *et al.*, 2009;
473 Baxter *et al.*, 2014; Choudhury *et al.*, 2017; Fichman and Mittler, 2020). Similarly, a multitude of

474 stress conditions in plants have been demonstrated to initiate or enhance autophagy (Bassham
475 *et al.*, 2006; Liu *et al.*, 2009; Signorelli *et al.*, 2019; Su *et al.*, 2020). Moreover, defects in
476 antioxidant proteins in Arabidopsis and Chlamydomonas contribute to uncontrolled ROS bursts
477 and autophagy induction (Pérez-Pérez *et al.*, 2012*a*; Shibata *et al.*, 2013). While the concurrent
478 induction of ROS production and autophagy activation suggests a positive correlation between
479 these cellular processes, certain molecular mechanisms have been reported in animal cells,
480 yeast, and Chlamydomonas, indicating that ROS could potentially exert a negative influence on
481 autophagy (Pérez-Pérez *et al.*, 2014, 2016; Frudd *et al.*, 2018). However, direct evidence of ROS-
482 mediated inhibition of autophagy remains scarce in plants. One of the fundamental unanswered
483 queries is whether a particular type of ROS functions as the primary messenger/modulator, if
484 any, to regulate autophagy. Our findings point in that direction, highlighting the differential
485 effects of ROS on autophagy and suggesting that, under specific stress conditions leading to a
486 highly oxidized cytoplasmic state, the autophagic process may be suppressed.
487 In this study, MV was used to specifically generate O_2^- and H_2O_2 in the chloroplast
488 (*revised in* Asada, 2006; Lascano *et al.*, 2012). Previous studies have reported the formation of
489 autophagosomes in root cells following incubation with MV (Xiong *et al.*, 2007*b*). Nevertheless,
490 our findings differ from these outcomes. It is important to acknowledge that certain variations
491 in experimental and methodological approaches between our research and the prior studies
492 may have a considerable impact on the interpretation of the outcomes. In the earlier studies,
493 MV treatments were administered on solid MS media, subjecting plants to 10 µM MV for a
494 duration of two days, and the observations were made in roots (heterotrophic tissues where
495 MV produces O_2^- and H_2O_2 in mitochondria). Conversely, in our study, MS liquid media was
496 supplemented with 1 µM MV, and leaves were analyzed (tissues where MV generates O_2^- and
497 H_2O_2 in chloroplast). Furthermore, a critical distinction lies in the method employed for
498 quantifying autophagosomes. Previous investigations employed monodansylcadaverine (MDC)
499 staining to identify acidic compartments. However, experiments involving autophagy-deficient
500 *atg* mutants, as well as co-localization analysis in GFP-ATG8 plants, indicated that the MDC-
501 stained structures do not clearly manifest as autophagosomes and/or autolysosomes
502 (Merkulova et al., 2014). In contrast, we used GFP-ATG8 plants for autophagy analysis through
503 confocal microscopy and western blot analysis, which are more reliable and widely accepted
504 method for identifying autophagosomes/autophagic bodies and monitoring autophagic activity
505 in general.
506 The relationship between autophagy and ROS is intricate, and our findings revealed that
507 different types of ROS, even when generated in the same organelle, can have different effects
508 on the autophagic process. We observed that under conditions of nutritional starvation, which
509 are canonical inducers of autophagy, oxidative treatments with MV and H_2O_2 had an inhibitory
510 effect on the autophagic flux (Fig. 2). This implies that the comparatively limited autophagosome
511 biogenesis rate under optimal growth conditions could potentially account for the absence of
512 observable inhibitory effects of ROS on autophagy in prior *in vivo* plant studies (Fig. 1). Opposite
513 to the inhibitory effects of H_2O_2 on the autophagic flux, the specific generation of $^1O_2$ in the *flu*
514 mutant plants, as well as treatments with DCMU and MB (Fufezan *et al.*, 2002; Op Den Camp *et*
515 *al.*, 2003; Flors *et al.*, 2006; Shao *et al.*, 2007, 2013; Dmitrieva *et al.*, 2020), increased the
516 autophagic activity (Fig. 4 and Fig. 5). These findings are consistent with previous research
517 demonstrating that treatments with norflurazon, an inhibitor of carotenoid biosynthesis,
518 triggers autophagy in *Chlamydomonas reinhardtii* (Pérez-Pérez *et al.*, 2016). Similarly to what is
519 observed in *flu* mutants (Op Den Camp *et al.*, 2003), norflurazon treatments lead to
520 perturbations in plastid homeostasis that increase the photosensitizing activity of tetrapyrroles,
521 which can transfer the excitation energy to the oxygen molecule, thereby generating $^1O_2$ (Kim

522 and Apel, 2013). Singlet oxygen, carotenoid derivatives, and tetrapyrroles are principal
523 components of the retrograde signaling pathway, a key process that regulates not only
524 chloroplastic processes but also intersects with other cellular signaling events playing broader
525 roles in plant function (Chan *et al.*, 2016).
526 With a shorter half-life and inability to cross membranes, the activity of $^1O_2$ is confined
527 to the thylakoid membrane of chloroplasts (Dmitrieva *et al.*, 2020). These characteristics provide
528 potential explanations for the absence of observable effects on the cytoplasmic redox state in
529 treatments involving DCMU, MB, and *flu* mutant plants (Fig. 4 and Fig. 5). Conversely, treatments
530 with MV and H_2O_2 highly oxidized the cytoplasmic redox state (Fig. 1 and Fig. 2). These results
531 establish a well-defined correlation between the cytoplasmic redox state of the cytoplasm and
532 autophagic activity.
533 The observation that the inhibition of autophagic flux and the oxidation of the
534 cytoplasmic redox state in MV treatments can be prevented by ROS scavengers such as tiron or
535 benzoic acid, as well as by treatment with the disulfide bonds reductant DTT, strengthens the
536 notion that H_2O_2 inhibits autophagy, but also suggests that protein oxidation in the cytoplasm
537 may be involved in this response. Notably, it has been proposed that proteins are the primary
538 targets of reactive oxidants and other radicals *in vivo* (Davies, 2005). At the molecular level, the
539 activity of certain ATG proteins has been shown to be regulated by redox changes. For instance,
540 ATG4, a protein involved in the cleavage of ATG8 for its lipidation and de-lipidation, is inhibited
541 by H_2O_2 in yeast and the green alga *Chlamydomonas reinhardtii* (Pérez-Pérez *et al.*, 2014, 2016).
542 Conversely, reducing agents such as DTT can restore the activity of ATG4 (Pérez-Pérez *et al.*,
543 2014, 2016). Furthermore, it has been reported in animal cells that oxidation of ATG3 and ATG7
544 leads to the inhibition of autophagy (Frudd *et al.*, 2018). The conservation of amino acid
545 sequence between the isoforms from yeast, human cells, and Arabidopsis (Fig. S3 and S4)
546 suggest that this type of regulation could also occur in plants.
547 The complexity of the relationship between autophagy and ROS becomes even more
548 complex when considering that this catabolic process is involved in the degradation of proteins
549 and oxidized organelles, which are primary sources of ROS production. The increased autophagic
550 flux observed during the recovery period after exposure to oxidative stress, accompanied by the
551 restoration of a reduced redox state in the cytoplasm, indicated that the inhibition of autophagy
552 by ROS is transient (Fig. 3). Through the assessment of autophagic flux, our objective was to
553 illuminate the role of autophagy in cellular adaptation to oxidative stress and its potential
554 involvement in stress recovery mechanisms. Our findings imply that inducing autophagy once
555 the oxidative stress has subsided is linked to the intracellular clearance of cytoplasmic
556 components damaged during oxidative stress. This is supported by experiments with the
557 antioxidants tiron and benzoic acid, which regulated ROS production and thwarted cell injury
558 (Fig. S2). These observations underscore the dynamic nature of autophagy in response to
559 oxidative stress and its subsequent recovery, pointing towards a complex regulatory mechanism
560 in Arabidopsis.
561 In summary, our work provides a novel perspective on the relationship between ROS
562 and autophagy. The fact that the generation of H_2O_2 and $^1O_2$ have different effects on autophagy
563 imply that the term "ROS" encompasses molecules with the ability to modulate this process in
564 distinct ways. Further studies are needed to unravel the molecular mechanisms underlying the
565 differential modulation of autophagy by ROS, being ATG4, ATG3 and ATG7 possible targets to
566 be oxidatively regulated.
567
568
569

570 **SUPPLEMENTARY DATA**

571 Supplementary Figure 1: Optimization of methyl viologen (MV) and H_2O_2
572 concentrations, and calibration of the redox sensors. Supplementary Figure 2: DTT, tiron
573 and benzoic acid reversed the effects of MV treatments.
574 Supplementary Figure 3: Sequence alignment of ATG4 proteases from different organisms.
575 Supplementary Figure 4: Sequence alignment of ATG3 and ATG7 proteins from different
576 organisms.
577 Supplementary Figure 5: Characterization of *fc2* and *flu* mutant plants under continuous light
578 conditions.
579 Supplementary Figure 6: Transcript level of *Atg* genes in Arabidopsis plants subjected to
580 different oxidative treatments.
581

582 **ACKNOWLEDGEMENTS**

583 We thank Dr. Leandro Ortega and Dr. Virginia Lobatto (Unidad de Doble Dependencia INTA-
584 CONICET (UDEA)) for helpful support with the confocal microscopy and for technical support,
585 respectively. We also thank Sistema Nacional de Microscopia of the Ministerio de Ciencia,
586 tecnología e innovación Productiva (MINCyT), Argentina.
587

588 **AUTHOR CONTRIBUTION:**

589 GR and RL: conceptualization; GR and AE: investigation; GR, AE, LS and RL: formal analysis; GR,
590 LS, and RL: resources; GR and AE: writing original draft and incorporated feedback from all
591 authors; GR and AE: visualization; GR and RL: supervision; GR, LS and RL: funding acquisition.
592

593 **CONFLICT OF INTEREST**

594 No conflict of interest declared.
595

596 **FUNDING**

597 This work was supported by grants from Agencia Nacional de Promoción Científica y
598 Tecnológica, Argentina: FONCYT-PICT-2019-0533 (RL), FONCyT PICT-2017-2863 (GR), and
599 FONCyT PICT-2020-2482 (LS); Consejo Nacional de Investigaciones Científicas y Técnicas
600 CONICET-PIP2015-PIP2019 (RL), Proyecto INTA 2019-PD-E6-I116-001 (RL and GR), and
601 Proyectos Consolidar, Secretaría de Ciencia y Técnica de la Universidad Nacional de Córdoba
602 (UNC) (RL).
603

604 **REFERENCES**

605 **Agbemafle W, Wong MM, Bassham DC**. 2023. Transcriptional and post-translational
606 regulation of plant autophagy. Journal of Experimental Botany **74**, 6006–6022.
607 **Aller I, Rouhier N, Meyer AJ**. 2013. Development of roGFP2-derived redox probes for
608 measurement of the glutathione redox potential in the cytosol of severely glutathione-
609 deficient rml1 seedlings. Frontiers in Plant Science **4**, 1–12.
610 **Apel K, Hirt H**. 2004. Reactive oxygen species: metabolism, oxidative stress, and signal
611 transduction. Annual review of plant biology **55**, 373–99.
612 **Asada K**. 2006. Production and Scavenging of Reactive Oxygen Species in Chloroplasts and
613 Their Functions. Plant Physiology **141**, 391–396.
614 **Bassham DC, Laporte M, Marty F, Moriyasu Y, Ohsumi Y, Olsen LJ, Yoshimoto K**. 2006.
615 Autophagy in Development and Stress Responses of Plants. Autophagy **2**, 2–11.
616 **Baxter A, Mittler R, Suzuki N**. 2014. ROS as key players in plant stress signalling. Journal of
617 experimental botany **65**, 1229–1240.
618 **Bechtold U, Richard O, Zamboni A, Gapper C, Geisler M, Pogson B, Karpinski S, Mullineaux**

619 **PM**. 2008. Impact of chloroplastic- and extracellular-sourced ROS on high light-responsive gene
620 expression in Arabidopsis. Journal of experimental botany **59**, 121–33.
621 **Breeze E, Harrison E, McHattie S, *et al.*** 2011. High-resolution temporal profiling of transcripts
622 during Arabidopsis leaf senescence reveals a distinct chronology of processes and regulation.
623 Plant Cell **23**, 873–894.
624 **Breusegem F Van, Dat JF**. 2006. Reactive Oxygen Species in Plant Cell Death. Plant physiology
625 **141**, 384–390.
626 **Breusegem F Van, Vranova E, Dat JF, Inze D**. 2001. The role of active oxygen species in plant
627 signal transduction. Plant Science **161**, 405–414.
628 **Chan KX, Phua SY, Crisp P, McQuinn R, Pogson BJ**. 2016. Learning the Languages of the
629 Chloroplast: Retrograde Signaling and beyond. Annual Review of Plant Biology **67**, 25–53.
630 **Choudhury FK, Rivero RM, Blumwald E, Mittler R**. 2017. Reactive oxygen species, abiotic
631 stress and stress combination. Plant Journal **90**, 856–867.
632 **Davies MJ**. 2005. The oxidative environment and protein damage. Biochimica et Biophysica
633 Acta - Proteins and Proteomics **1703**, 93–109.
634 **Dmitrieva VA, Tyutereva E V., Voitsekhovskaja O V.** 2020. Singlet oxygen in plants:
635 Generation, detection, and signaling roles. International Journal of Molecular Sciences **21**.
636 **Doelling JH, Walker JM, Friedman EM, Thompson AR, Vierstra RD**. 2002. The APG8/12-
637 activating enzyme APG7 is required for proper nutrient recycling and senescence in
638 Arabidopsis thaliana. Journal of Biological Chemistry **277**, 33105–33114.
639 **Fales FW**. 1951. The assimilation and degradation of carbohydrates by yeast cells. The Journal
640 of biological chemistry **193**, 113–124.
641 **Farrington JA, Ebert M, Land EJ, Fletcher K**. 1973. Bipyridylium quaternary salts and related
642 compounds. V. Pulse radiolysis studies of the reaction of paraquat radical with oxygen.
643 Implications for the mode of action of bipyridyl herbicides. Biochimica et Biophysica Acta **314**,
644 372–381.
645 **Feng Y, Yao Z, Klionsky DJ**. 2015. How to control self-digestion: transcriptional, post-
646 transcriptional, and post-translational regulation of autophagy. Trends in cell biology **25**, 354–
647 363.
648 **Fernandez-göbel TF, Deanna R, Muñoz NB, Robert G, Asurmendi S, Lascano R**. 2019. Redox
649 Systemic Signaling and Induced Tolerance Responses During Soybean – Bradyrhizobium
650 japonicum Interaction : Involvement of Nod Factor Receptor and Autoregulation of
651 Nodulation. Frontiers in Plant Science **10**, 1–15.
652 **Fichman Y, Mittler R**. 2020. Rapid systemic signaling during abiotic and biotic stresses: is the
653 ROS wave master of all trades? Plant Journal **102**, 887–896.
654 **Flors C, Fryer MJ, Waring J, Reeder B, Bechtold U, Mullineaux PM, Nonell S, Wilson MT,**
655 **Baker NR**. 2006. Imaging the production of singlet oxygen in vivo using a new fluorescent
656 sensor, Singlet Oxygen Sensor Green. Journal of experimental botany **57**, 1725–34.
657 **Foyer CH, Hanke G**. 2022. ROS production and signalling in chloroplasts: cornerstones and
658 evolving concepts. Plant Journal **111**, 642–661.
659 **Foyer CH, Noctor G**. 2009. Redox Regulation in Photosynthetic Organisms: signaling,
660 acclimation, and practical implications. Antioxidants & Redox Signaling **11**, 861–905.
661 **Foyer CH, Noctor G**. 2011*a*. Ascorbate and glutathione: the heart of the redox hub. Plant
662 physiology **155**, 2–18.
663 **Foyer CH, Noctor G**. 2011*b*. Ascorbate and glutathione: the heart of the redox hub. Plant
664 physiology **155**, 2–18.
665 **Frudd K, Burgoyne T, Burgoyne JR**. 2018. Oxidation of Atg3 and Atg7 mediates inhibition of
666 autophagy. Nature Communications **9**, 1–15.
667 **Fufezan C, Rutherford AW, Krieger-liszkay A**. 2002. Singlet oxygen production in herbicide-
668 treated photosystem II. FEBS **532**, 407–410.
669 **Hanaoka H, Noda T, Shirano Y, Kato T, Hayashi H, Shibata D, Tabata S, Ohsumi Y**. 2002. Leaf
670 senescence and starvation-induced chlorosis are accelerated by the disruption of an

671 Arabidopsis autophagy gene. Plant Physiol **129**, 1181–1193.
672 **Heath RL, Packer L**. 1968. Photoperoxidation in isolated chloroplasts. Archives of Biochemistry
673 and Biophysics **125**, 189–198.
674 **Izumi M, Ishida H, Nakamura S, Hidema J**. 2017. Entire Photodamaged Chloroplasts Are
675 Transported to the Central Vacuole by Autophagy. The Plant Cell **29**, 377.
676 **Karpinski S, Reynolds H, Karpinska B, Wingsle G, Creissen G, Mullineaux P**. 1999. Systemic
677 signaling and acclimation in response to excess excitation energy in Arabidopsis. Science **284**,
678 654–7.
679 **Kim C, Apel K**. 2013. 1O2-mediated and EXECUTER-dependent retrograde plastid-to-nucleus
680 signaling in norflurazon-treated seedlings of arabidopsis thaliana. Molecular Plant **6**, 1580–
681 1591.
682 **Lascano R, Munoz N, Robert G, Rodriguez M, Melchiorre M, Trippi V, Quero G**. 2012.
683 Paraquat: An Oxidative Stress Inducer. Herbicides - Properties, Synthesis and Control of
684 Weeds. London: IntechOpen, 135–148.
685 **Lemke MD, Fisher KE, Kozlowska MA, Tano DW, Woodson JD**. 2021. The core autophagy
686 machinery is not required for chloroplast singlet oxygen - mediated cell death in the
687 Arabidopsis thaliana plastid ferrochelatase two mutant. BMC plant biology **21**, 1–20.
688 **Liu Y, Xiong Y, Bassham DC**. 2009. Autophagy is required for tolerance of drought and salt
689 stress in plants. Autophagy **5**, 954–63.
690 **Liubimovskii SO, Ustynyuk LY, Tikhonov AN**. 2021. Superoxide radical scavenging by sodium
691 4,5-dihydroxybenzene-1,3-disulfonate dissolved in water: Experimental and quantum chemical
692 studies. Journal of Molecular Liquids **333**, 20–23.
693 **Livak KJ, Schmittgen TD**. 2001. Analysis of relative gene expression data using real-time
694 quantitative PCR and the 2(-Delta Delta CT) Method. Methods **25**, 402–408.
695 **Mansouri A, Makris DP, Kefalas P**. 2005. Determination of hydrogen peroxide scavenging
696 activity of cinnamic and benzoic acids employing a highly sensitive peroxyoxalate
697 chemiluminescence-based assay: Structure-activity relationships. Journal of Pharmaceutical
698 and Biomedical Analysis **39**, 22–26.
699 **Masclaux-Daubresse C, Clement G, Anne P, Routaboul J-M, Guiboileau A, Soulay F, Shirasu K,**
700 **Yoshimoto K**. 2014. Stitching together the Multiple Dimensions of Autophagy Using
701 Metabolomics and Transcriptomics Reveals Impacts on Metabolism, Development, and Plant
702 Responses to the Environment in Arabidopsis. The Plant Cell **26**, 1857–1877.
703 **Mehler AH**. 1951. Studies on reactions of illuminated chloroplasts. II. Stimulation and
704 inhibition of the reaction with molecular oxygen. Archives of Biochemistry and Biophysics **34**,
705 339–351.
706 **Melchiorre M, Robert G, Trippi V, Racca R, Lascano HR**. 2009. Superoxide dismutase and
707 glutathione reductase overexpression in wheat protoplast: photooxidative stress tolerance and
708 changes in cellular redox state. Plant Growth Regulation **57**, 57–68.
709 **Meskauskiene R, Nater M, Goslings D, Kessler F, Op den Camp R, Apel K**. 2001. FLU: A
710 negative regulator of chlorophyll biosynthesis in arabidopsis thaliana. Proceedings of the
711 National Academy of Sciences of the United States of America **98**, 12826–12831.
712 **Miller G, Schlauch K, Tam R, Cortes D, Torres MA, Shulaev V, Dangl JL, Mittler R**. 2009. The
713 plant NADPH oxidase RBOHD mediates rapid systemic signaling in response to diverse stimuli.
714 Science Signaling **2**.
715 **Munch D, Rodriguez E, Bressendorff S, Park OK, Hofius D, Petersen M**. 2014. Autophagy
716 deficiency leads to accumulation of ubiquitinated proteins, ER stress, and cell death in
717 Arabidopsis. Autophagy **10**, 1579–1587.
718 **Muñoz N, Robert G, Melchiorre M, Racca R, Lascano R**. 2012. Saline and osmotic stress
719 differentially affects apoplastic and intracellular reactive oxygen species production, curling
720 and death of root hair during Glycine max L.-Bradyrhizobium japonicum interaction.
721 Environmental and Experimental Botany **78**, 76–83.
722 **Nakamura S, Hidema J, Sakamoto W, Ishida H, Izumi M**. 2018. Selective Elimination of

Membrane-Damaged Chloroplasts via microautophagy. Plant Physiology **177**, 1007–1026.
Navabpour S, Morris K, Allen R, Harrison E, A-H-Mackerness S, Buchanan-Wollaston V. 2003. Expression of senescence-enhanced genes in response to oxidative stress. Journal of experimental botany **54**, 2285–92.
Nazish T, Huang YJ, Zhang J, Xia JQ, Alfatih A, Luo C, Cai XT, Xi J, Xu P, Xiang C Bin. 2022. Understanding paraquat resistance mechanisms in Arabidopsis thaliana to facilitate the development of paraquat-resistant crops. Plant Communications **3**, 1–11.
Nietzel T, Elsässer M, Ruberti C, *et al.* 2019. The fluorescent protein sensor roGFP2-Orp1 monitors in vivo H 2 O 2 and thiol redox integration and elucidates intracellular H 2 O 2 dynamics during elicitor-induced oxidative burst in Arabidopsis. New Phytologist **221**, 1649–1664.
Oikawa K, Goto-yamada S, Hayashi Y, *et al.* 2022. Pexophagy suppresses ROS-induced damage in leaf cells under high-intensity light.
Op Den Camp RGL, Przybyla D, Ochsenbein C, *et al.* 2003. Rapid Induction of Distinct Stress Responses after the Release of Singlet Oxygen in Arabidopsis. Plant Cell **15**, 2320–2332.
Peláez-vico MÁ, Fichman Y, Zandalinas SI, Van F, Karpiński SM, Mittler R. 2022. ROS and redox regulation of cell-to-cell and systemic signaling in plants during stress. Free Radical Biology and Medicine.
Pérez-Pérez ME, Couso I, Crespo JL. 2012*a*. Carotenoid deficiency triggers autophagy in the model green alga Chlamydomonas reinhardtii. Autophagy **8**, 376–388.
Pérez-Pérez ME, Lemaire SD, Crespo JL. 2012*b*. Reactive oxygen species and autophagy in plants and algae. Plant physiology **160**, 156–64.
Pérez-Pérez ME, Lemaire SD, Crespo JL. 2016. Control of Autophagy in *Chlamydomonas* Is Mediated through Redox-Dependent Inactivation of the ATG4 Protease. Plant Physiology **172**, 2219–2234.
Pérez-Pérez ME, Zaffagnini M, Marchand CH, Crespo JL, Lemaire SD. 2014. The yeast autophagy protease Atg4 is regulated by thioredoxin. Autophagy **10**, 1–12.
Qi H, Xia FN, Xiao S. 2021. Autophagy in plants: Physiological roles and post-translational regulation. Journal of Integrative Plant Biology **63**, 161–179.
Di Rienzo JA, Guzmán AW, Casanoves F. 2002. A multiple-comparisons method based on the distribution of the root node distance of a binary tree. Journal of Agricultural, Biological, and Environmental Statistics **7**, 129–142.
Robert G, Melchiorre M, Racca R, Trippi V, Lascano HR. 2009. Apoplastic superoxide level in wheat protoplast under photooxidative stress is regulated by chloroplast redox signals : Effects on the antioxidant system. Plant Science **177**, 168–174.
Robert G, Muñoz N, Alvarado-Affantranger X, Saavedra L, Davidenco V, Rodríguez-Kessler M, Estrada-Navarrete G, Sánchez F, Lascano R. 2018. Phosphatidylinositol 3-kinase function at very early symbiont perception: A local nodulation control under stress conditions? Journal of Experimental Botany **69**, 2037–2048.
Robert G, Muñoz N, Melchiorre M, Sánchez F, Lascano R. 2014. Expression of animal anti-apoptotic gene Ced-9 enhances tolerance during Glycine max L.-Bradyrhizobium japonicum interaction under saline stress but reduces nodule formation. PLoS One **9**, e101747.
Robert G, Yagyu M, Koizumi T, Naya L, Masclaux-Daubresse C, Yoshimoto K. 2021. Ammonium stress increases microautophagic activity while impairing macroautophagic flux in Arabidopsis roots. Plant Journal **105**, 1083–1097.
Rubin G, Tohge T, Matsuda F, Saito K, Scheible W-R. 2009. Members of the LBD Family of Transcription Factors Repress Anthocyanin Synthesis and Affect Additional Nitrogen Responses in Arabidopsis. The Plant Cell **21**, 3567–3584.
Scarpeci TE, Zanor MI, Carrillo N, Mueller-Roeber B, Valle EM. 2008. Generation of superoxide anion in chloroplasts of Arabidopsis thaliana during active photosynthesis : a focus on rapidly induced genes. Plant Mol Biol **66**, 361–378.
Scharfenberg M, Mittermayr L, Von Roepenack-Lahaye E, Schlicke H, Grimm B, Leister D,

775 **Kleine T**. 2015. Functional characterization of the two ferrochelatases in Arabidopsis thaliana.
776 Plant Cell and Environment **38**, 280–298.
777 **Schwarzländer M, Dick TP, Meye AJ, Morgan B**. 2015. Dissecting Redox Biology using
778 Fluorescent Protein Sensors. Antioxidants & Redox Signaling **00**, 150413084017007.
779 **Schwarzländer M, Dick TP, Meyer AJ, Morgan B**. 2016. Dissecting redox biology using
780 fluorescent protein sensors. Antioxidants and Redox Signaling **24**, 680–712.
781 **Schwarzlander M, Fricker MD, Muller C, Marty L, Brach T, Novak J, Sweetlove LJ, Hell R,**
782 **Meyer AJ**. 2008. Confocal imaging of glutathione redox potential in living plant cells. Journal of
783 Microscopy **231**, 299–316.
784 **Schwarzländer M, Fricker MD, Sweetlove LJ**. 2009. Monitoring the in vivo redox state of plant
785 mitochondria: effect of respiratory inhibitors, abiotic stress and assessment of recovery from
786 oxidative challenge. Biochimica et biophysica acta **1787**, 468–75.
787 **Shao N, Duan GY, Bock R, Molekulare M**. 2013. A Mediator of Singlet Oxygen Responses in
788 Chlamydomonas reinhardtii and Arabidopsis Identi fi ed by a Luciferase-Based Genetic Screen
789 in Algal Cells. The Plant Cell **25**, 4209–4226.
790 **Shao N, Krieger-liszkay A, Schroda M, Beck CF**. 2007. A reporter system for the individual
791 detection of hydrogen peroxide and singlet oxygen : its use for the assay of reactive oxygen
792 species produced in vivo. The Plant journal **50**, 475–487.
793 **Shibata M, Oikawa K, Yoshimoto K, Kondo M, Mano S, Yamada K, Hayashi M, Sakamoto W,**
794 **Ohsumi Y, Nishimura M**. 2013. Highly Oxidized Peroxisomes Are Selectively Degraded via
795 Autophagy in Arabidopsis. The Plant cell **25**, 4967–83.
796 **Signorelli S, Tarkowski ŁP, Van den Ende W, Bassham DC**. 2019. Linking Autophagy to Abiotic
797 and Biotic Stress Responses. Trends in Plant Science **24**, 413–430.
798 **Su T, Li X, Yang M, Shao Q, Zhao Y, Ma C, Wang P**. 2020. Autophagy: An Intracellular
799 Degradation Pathway Regulating Plant Survival and Stress Response. Frontiers in Plant Science
800 **11**, 1–16.
801 **Trippi VS, Lascano HR, Melchiorre M**. 2009. Plant senescence: A self-induced process. Current
802 topics in plant biology **10**, 1–15.
803 **Velika B, Kron I**. 2012. Antioxidant properties of benzoic acid derivatives against Superoxide
804 radical. Free Radicals and Antioxidants **2**, 62–67.
805 **Wang P, Wang T, Han J, Li M, Zhao Y, Su T, Ma C**. 2021. Plant Autophagy : An Intricate Process
806 Controlled by Various Signaling Pathways. Frontiers in Plant Science **12**, 754982.
807 **Willems P, Mhamdi A, Stael S, Storme V, Kerchev P, Noctor G, Gevaert K, Van Breusegem F**.
808 2016. The ROS wheel: Refining ROS transcriptional footprints. Plant Physiology **171**, 1720–
809 1733.
810 **Wintermans M. j. FG, De Mots A.** 1965. SPECTROPHOTOMETRIC CHARACTERISTICS OF
811 CHLOROPHYLLS a AND b AND THEIR PHEOPHYTINS IN ETHANOL. Biochimica et biophysica acta
812 **109**, 448–453.
813 **Woodson JD**. 2019. Chloroplast stress signals: regulation of cellular degradation and
814 chloroplast turnover. Current Opinion in Plant Biology **52**, 30–37.
815 **Xiong Y, Contento AL, Bassham DC**. 2007*a*. Disruption of Autophagy Results in Constitutive
816 Oxidative Stress in Arabidopsis. Autophagy **3**, 257–258.
817 **Xiong Y, Contento AL, Nguyen PQ, Bassham DC**. 2007*b*. Degradation of oxidized proteins by
818 autophagy during oxidative stress in Arabidopsis. Plant physiology **143**, 291–9.
819 **Yang M, Bu F, Huang W, Chen L**. 2019. Multiple regulatory levels shape autophagy activity in
820 plants. Frontiers in Plant Science **10**, 1–7.
821 **Yoshimoto K**. 2012. Beginning to understand autophagy, an intracellular self-degradation
822 system in plants. Plant & cell physiology **53**, 1355–65.
823 **Yoshimoto K, Hanaoka H, Sato S, Kato T, Tabata S, Noda T**. 2004. Processing of ATG8s ,
824 Ubiquitin-Like Proteins , and Their Deconjugation by ATG4s Are Essential for Plant Autophagy.
825 The Plant Cell **16**, 2967–2983.
826 **Yoshimoto K, Jikumaru Y, Kamiya Y, Kusano M, Consonni C, Panstruga R, Ohsumi Y, Shirasu**

827 **K**. 2009. Autophagy negatively regulates cell death by controlling NPR1-dependent salicylic
828 acid signaling during senescence and the innate immune response in Arabidopsis. The Plant
829 cell **21**, 2914–27.
830 **Yoshimoto K, Ohsumi Y**. 2018. Unveiling the molecular mechanisms of plant autophagy-from
831 autophagosomes to vacuoles in plants. Plant and Cell Physiology **59**, 1337–1344.
832 **Zandalinas SI, Fichman Y, Devireddy AR, Sengupta S, Azad RK, Mittler R**. 2020. Systemic
833 signaling during abiotic stress combination in plants. Proceedings of the National Academy of
834 Sciences **117**, 13810–13820.
835 **Zheng X, Yang Z, Gu Q, Xia F, Fu Y, Liu P, Yin XM, Li M**. 2020. The protease activity of human
836 ATG4B is regulated by reversible oxidative modification. Autophagy **16**, 1838–1850.
837 **Zhou J, Wang J, Cheng Y, Chi YJ, Fan B, Yu JQ, Chen Z**. 2013. NBR1-Mediated Selective
838 Autophagy Targets Insoluble Ubiquitinated Protein Aggregates in Plant Stress Responses. PLoS
839 Genetics **9**.
840 **Zhuang X, Cui Y, Gao C, Jiang L**. 2015. Endocytic and autophagic pathways crosstalk in plants.
841 Current Opinion in Plant Biology **28**, 39–47.
842
843 **Figure legends**

844 **Figure 1:** Autophagic flux and cytoplasmic redox state in *Arabidopsis thaliana* plants exposed to
845 different abiotic stress conditions. (A-C) Seven-day old 35S:GFP-ATG8a transgenic plants and
846 cytosol-targeted fluorescent redox sensors GFP2-Orp1 and GRX-roGFP2 expressing plants were
847 exposed to different stress conditions in MS liquid medium. To induce autophagic bodies
848 accumulation, MS liquid medium was supplemented with 1 µM Concanamycin A. (A)
849 Representative images showing autophagic bodies accumulation and cytoplasmic redox state.
850 The stress treatments were performed for 16 h, followed by the evaluation of autophagic bodies
851 accumulation (GFP-ATG8 columns) and the cytoplasmic redox state (GRX-roGFP and GFP2-Orp1
852 columns) by confocal microscopy. Arrowheads indicate some of the autophagic bodies
853 observed. Scale bars: 30 µm. GRX-roGFP and GFP2-Orp1 columns are ratiometric images. For
854 pseudocolor display, the ratio was coded on a spectral color scale ranging from blue (fully
855 reduced) to red (fully oxidized). The treatments included: MS with nitrogen (control), MS with
856 nitrogen in darkness (-C), MS without nitrogen (-N), MS with nitrogen supplemented with 100
857 mM mannitol (Manitol), 50 mM NaCl (NaCl), 1 µM methyl viologen (MV) and 10 mM H_2O_2. (B)
858 Average number of autophagic bodies accumulation per section. The average number of
859 autophagic bodies was calculated from single-plane confocal images. Two sections from at least
860 7 plants were analyzed. (C) Average of cytoplasmic redox state expressed as the ratio of the
861 fluorescence intensities measured at 488 nm and 405 nm. At least 6 plants were analyzed.
862 Statistically significant differences are indicated by asterisks (*$P < 0.05$; error bars: means ± SEM,
863 DGC test).
864
865

866 **Figure 2:** Treatments with MV and H_2O_2 oxidized the cytoplasmic redox state and prevented
867 autophagy induction in Arabidopsis. (A-C) Seven-day old 35S:GFP-ATG8a transgenic plants and
868 cytosol-targeted fluorescent redox sensors GFP2-Orp1 and GRX-roGFP2 expressing plants were
869 exposed to autophagy-inducing conditions and the effect of methyl viologen (MV) and H_2O_2 on
870 autophagic flux and cytoplasmic redox state were analyzed. (A) Representative images showing
871 autophagic bodies accumulation and cytoplasmic redox state. The stress treatments were
872 performed for 16 h, followed by the evaluation of autophagic bodies accumulation (GFP-ATG8
873 columns) and the cytoplasmic redox state (GRX-roGFP and GFP2-Orp1 columns) by confocal
874 microscopy. To induced autophagic bodies accumulation, MS liquid medium was supplemented
875 with 1 µM Concanamycin A. Arrowheads indicate some of the autophagic bodies observed. Scale
876 bars: 30 µm. GRX-roGFP and GFP2-Orp1 columns are ratiometric images. The treatments
877 included: MS with nitrogen (control), MS with nitrogen in darkness (-C) supplemented with 10

878 mM H_2O_2 (-C + H_2O_2), MS without nitrogen (-N) supplemented with 1 µM methyl viologen (-N +
879 MV) or 10 mM H_2O_2 (-N + H_2O_2). 10 mM Tiron and 10 mM Benzoic acid (BA) were used for ROS
880 scavenging (-N + MV + Tiron and -N + MV + BA). (B) Average of autophagic bodies accumulation
881 per section. The average of autophagic bodies number was calculated from single-plane confocal
882 images. Two sections from at least 6 plants were analyzed. (C) Average of cytoplasmic redox
883 state expressed as the ratio of the fluorescence intensities measured at 488 nm and 405 nm
884 from single-plane confocal images. At least 6 plants were analyzed. (D) Effects of oxidative
885 treatments on the autophagic flux evaluated through the degradation of the GFP-ATG8a fusion
886 protein by western blot. Seven-day old 35S:GFP-ATG8a transgenic Arabidopsis seedlings were
887 exposed to the different treatments for 6 h. The GFP-ATG8a fusion has a predicted molecular
888 weight of approximately 40 kDa (closed arrowheads); free GFP has a predicted molecular weight
889 of 27 kDa (open arrowheads). Representative images are shown. Ratio: the numbers in brackets
890 denote the GFP/GFP-ATG8 ratio relativized to the same condition without oxidative treatment.
891 Three replicates were performed (more than fifty plants per replicate). HL: high light treatment
892 (≈1000 µmoles m^{-2} s^{-1}). Asterisks indicate statistically significant differences (*P < 0.05; error
893 bars: means ± SEM, DGC test).
894
895
896 **Figure 3:** Autophagy is induced after oxidative stress treatments in Arabidopsis. (A-D) Seven-day
897 old transgenic plants expressing 35S:GFP-ATG8a and cytosol-targeted fluorescent redox sensors
898 GFP2-Orp1 and GRX-roGFP2 were subjected to a brief exposure of oxidative stress, either 10
899 mM H_2O_2 or high light intensity (≈1000 µmoles m^{-2} s^{-1}), for 4 h. Subsequently they were
900 transferred to MS liquid medium for a 20-hour recovery period under continuous light (120
901 µmoles m^{-2} s^{-1}) (recovery). Control plants were incubated under continuous light (120 µmoles m^{-2}
902 s^{-1}) in H_2O_2-free MS liquid medium for 24 h. Stressed plants were incubated in MS
903 supplemented with 10 mM H_2O_2 or high light intensity (≈1000 µmoles m^{-2} s^{-1}) for 24 h. (A)
904 Representative images showing autophagic bodies accumulation and cytoplasmic redox state.
905 To induce accumulation of autophagic bodies, MS liquid medium was supplemented with 1 µM
906 Concanamycin A. Arrowheads indicate some of the autophagic bodies observed. Scale bars: 30
907 µm. GRX-roGFP and GFP2-Orp1 columns represent ratiometric images, with pseudocolor display
908 indicating the ratio on a spectral color scale ranging from blue (fully reduced) to red (fully
909 oxidized). (B) Average number of autophagic bodies accumulation per section. The average
910 number of autophagic bodies was calculated from single-plane confocal images. Two sections
911 from at least 6 plants were analyzed. (C) Average cytoplasmic redox state expressed as the ratio
912 of the fluorescence intensities measured at 488 nm and 405 nm from single-plane confocal
913 images. At least 6 plants were analyzed. Asterisks indicate statistically significant differences (*P
914 < 0.05; error bars: means ± SEM, DGC test). (D) Autophagic flux evaluated through the
915 degradation of the GFP-ATG8a fusion protein by western blot. Total protein (40 µg) was
916 subjected to immunoblot analysis with anti-GFP antibodies. The GFP-ATG8a fusion has a
917 predicted molecular weight of approximately 40 kDa (closed arrowheads), while free GFP has a
918 predicted molecular weight of 27 kDa (open arrowheads). Representative images are shown.
919 The numbers in brackets denote the GFP/GFP-ATG8 ratio relativized to the control condition.
920 Three replicates were performed (n > 50 plants per replicate). Asterisks indicate statistically
921 significant differences (*P < 0.05; error bars: means ± SEM, DGC test).
922
923
924 **Figure 4:** DCMU and methylene blue treatments induced autophagic flux in Arabidopsis. (A-D)
925 Seven-day old transgenic plants expressing 35S:GFP-ATG8a and cytosol-targeted fluorescent
926 redox sensors GFP2-Orp1 and GRX-roGFP2 were incubated in MS medium supplemented with
927 either 20 µM 3-(3,4-dichlorophenyl)-1,1-dimethylurea (DCMU) or 20 µM methylene blue (MB),
928 and the autophagic flux and cytoplasmic redox state were evaluated. (A) Representative images

929 showing autophagic bodies accumulation and cytoplasmic redox state after 16 h of treatment.
930 To induce autophagic bodies accumulation, MS liquid medium was supplemented with 1 μM
931 Concanamycin A. Some of the autophagic bodies are indicated by arrowheads. Scale bars: 30
932 μm. The GRX-roGFP and GFP2-Orp1 columns represent ratiometric images. For pseudo color
933 display, the ratio was coded using a spectral color scale ranging from blue (fully reduced) to red
934 (fully oxidized). (B) Average number of autophagic bodies per section. The average number of
935 autophagic bodies was calculated from single-plane confocal images. Two sections from at least
936 5 plants were analyzed. (C) Average cytoplasmic redox state expressed as the ratio of the
937 fluorescence intensities measured at 488 nm and 405 nm from single-plane confocal images.
938 Analysis was performed on at least 4 plants. Asterisks indicate statistically significant differences
939 (*$P < 0.05$; error bars: means ± SEM, DGC test). (D) Evaluation of the effects of DCMU and MB
940 on autophagic flux through degradation of the GFP-ATG8a fusion protein by western blot. Seven-
941 day old transgenic Arabidopsis seedlings expressing 35S:GFP-ATG8a were exposed to the
942 different treatments for 6 h. Total protein (40 μg) was subjected to immunoblot analysis with
943 anti-GFP antibodies. The GFP-ATG8a fusion has a predicted molecular weight of approximately
944 40 kDa (closed arrowheads), while free GFP has a predicted molecular weight of 27 kDa (open
945 arrowheads). Representative images are shown. The numbers in brackets denote the GFP/GFP-
946 ATG8 ratio relative to the control condition. Four replicates were performed with more than
947 fifty plants per replicate. (E) Seven-day old Arabidopsis seedlings were exposed to the different
948 treatments for 6 h and soluble sugar content was analyzed. FW: fresh weight. Asterisks indicate
949 statistically significant differences (*$P < 0.05$; error bars: means ± SEM, DGC test).

950

951 **Figure 5:** Autophagic flux is induced in conditionally chloroplast 1O2-hyperproducing *flu* mutant
952 Arabidopsis plants. (A-C) Seven-day old wildtype (Col-0) and *flu* mutant plants expressing
953 35S:GFP-ATG8a or GFP2-Orp1 were transferred to darkness for 8 h, followed by re-exposure to
954 light. Control plants were maintained under continuous light conditions. After 8 h, the
955 autophagic flux and cytoplasmic redox state were analyzed. (A) Representative images showing
956 autophagic bodies accumulation and cytoplasmic redox state. To induce autophagic bodies
957 accumulation, the MS liquid medium was supplemented with 1 μM Concanamycin A. The GFP2-
958 Orp1 columns represent ratiometric images. For pseudocolor display, the ratio was coded on a
959 spectral color scale ranging from blue (fully reduced) to red (fully oxidized). Arrowheads indicate
960 some of the autophagic bodies observed. Scale bars: 30 μm. (B) Average number of autophagic
961 bodies accumulation per section. The average number of autophagic bodies was calculated from
962 single-plane confocal images. Two different sections from at least 6 plants were analyzed. (C)
963 Average cytoplasmic redox state expressed as the ratio of the fluorescence intensities measured
964 at 405 nm and 488 nm from single-plane confocal images. At least 4 plants were analyzed.
965 Asterisks indicate statistically significant differences (*$P < 0.05$; error bars: means ± SEM, DGC
966 test). (D) Evaluation of autophagic flux through the degradation of the GFP-ATG8a fusion protein
967 by western blot. Seven-day old wildtype (Col-0) and *flu* mutant plants expressing 35S:GFP-ATG8a
968 were transferred to darkness for 8 h and then re-exposed to light for 6 h (after darkness).
969 Continuous light was used as a control (light). Total protein (40 μg) was subjected to immunoblot
970 analysis with anti-GFP antibodies. The GFP-ATG8a fusion has a predicted molecular weight of
971 approximately 40 kDa (closed arrowheads); while free GFP has a predicted molecular weight of
972 27 kDa (open arrowheads). Representative images are shown. The numbers in brackets denote
973 the GFP/GFP-ATG8 ratio relative to *flu* mutans under control condition. Three replicates were
974 performed (more than fifty plants per replicate). Asterisks indicate statistically significant
975 differences.
976
977

978 **FIGURE 1**

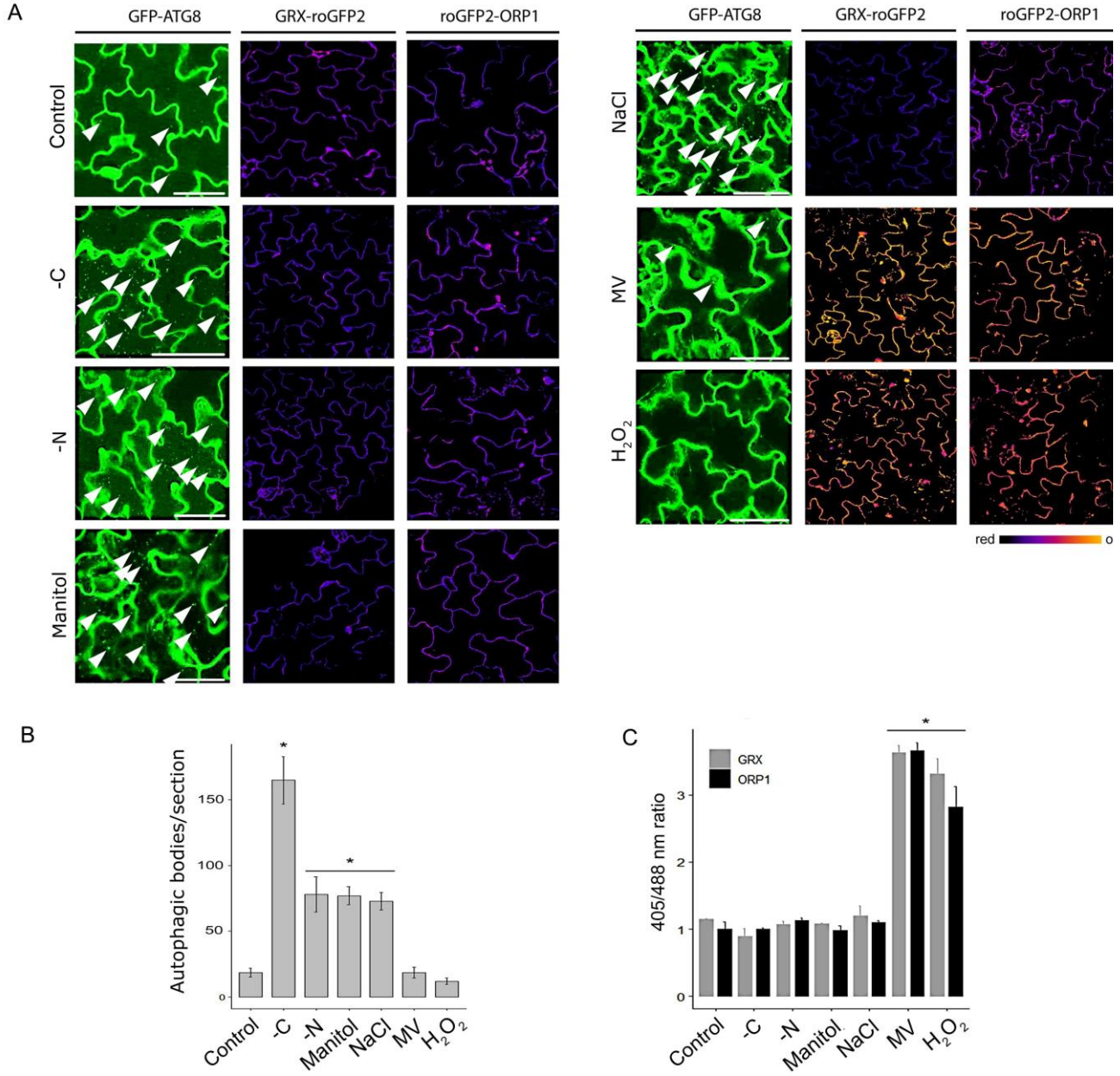

979

980

981

982

983

984

985 **FIGURE 2**

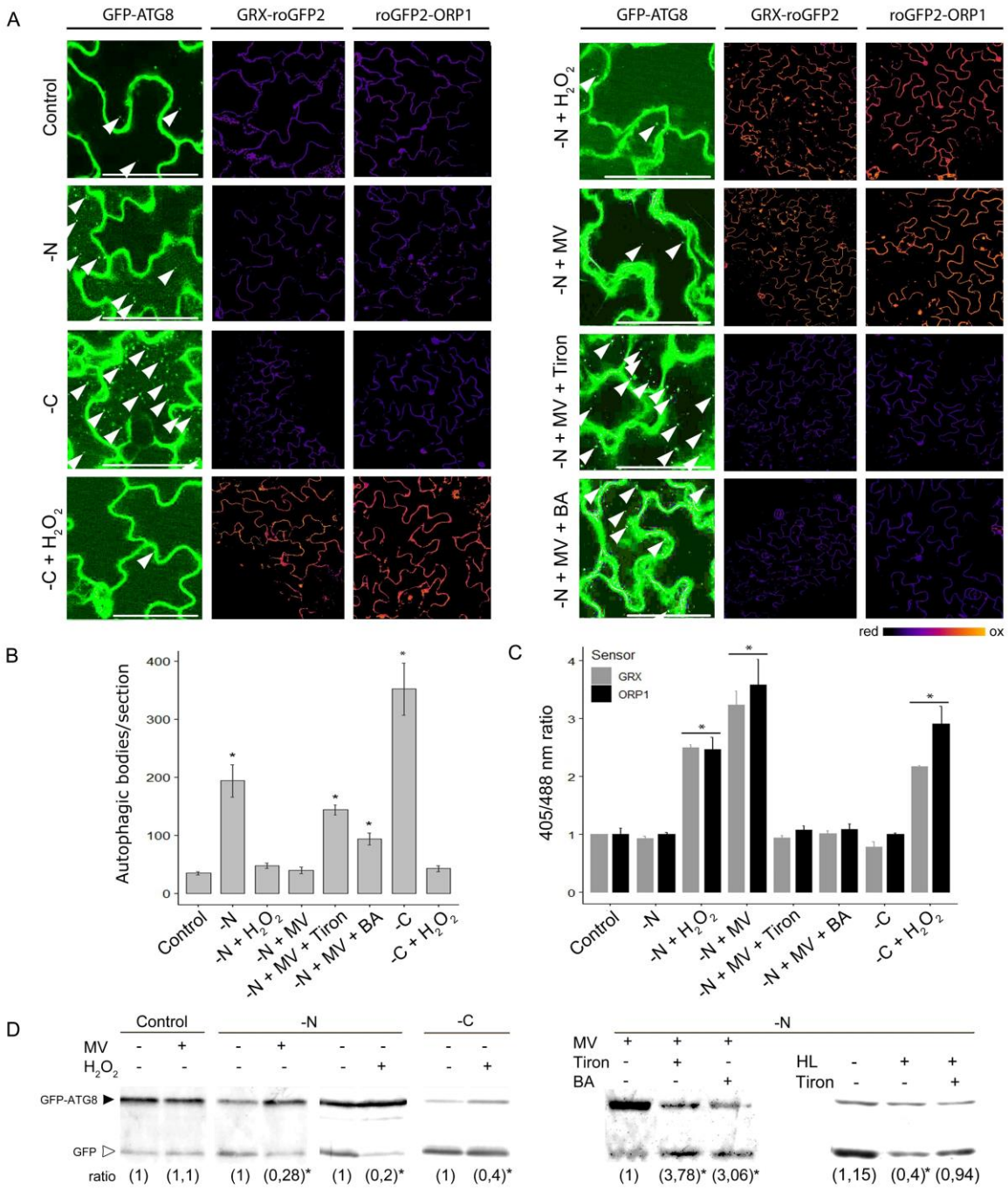

986

987

988

989

990

991

992 **FIGURE 3**

993

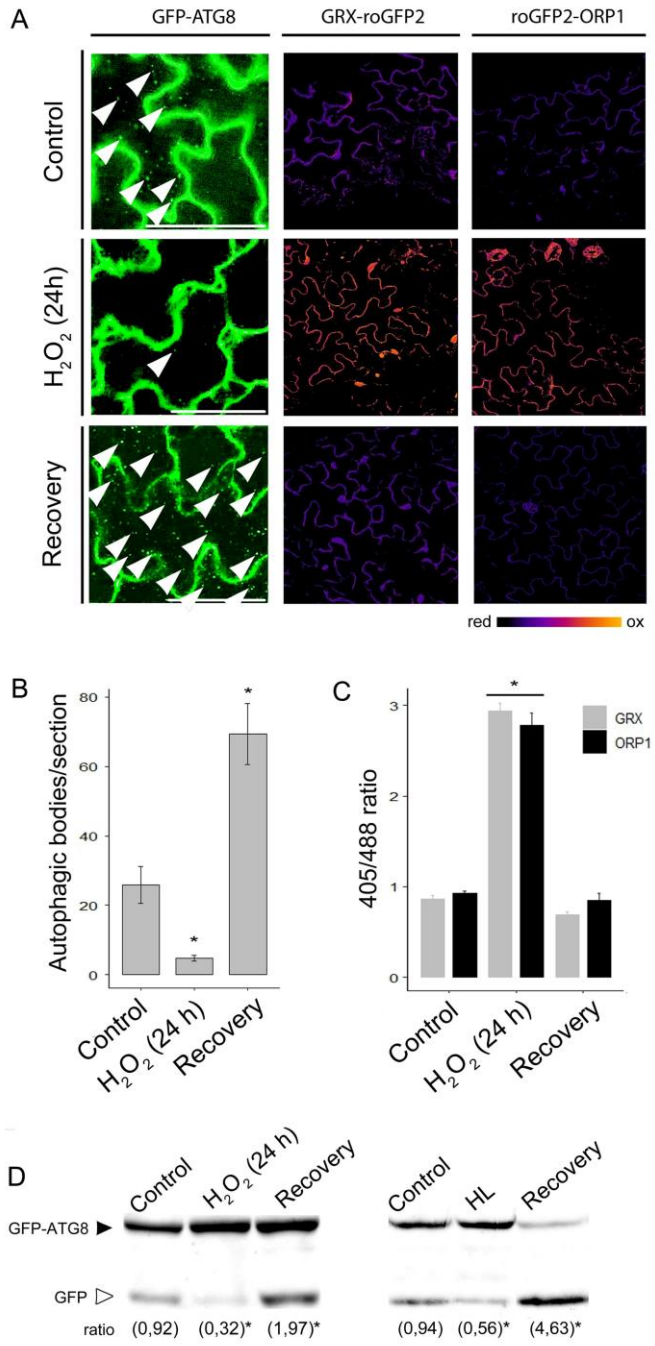

994
995
996
997
998
999
1000
1001

1002 **FIGURE 4**

1003

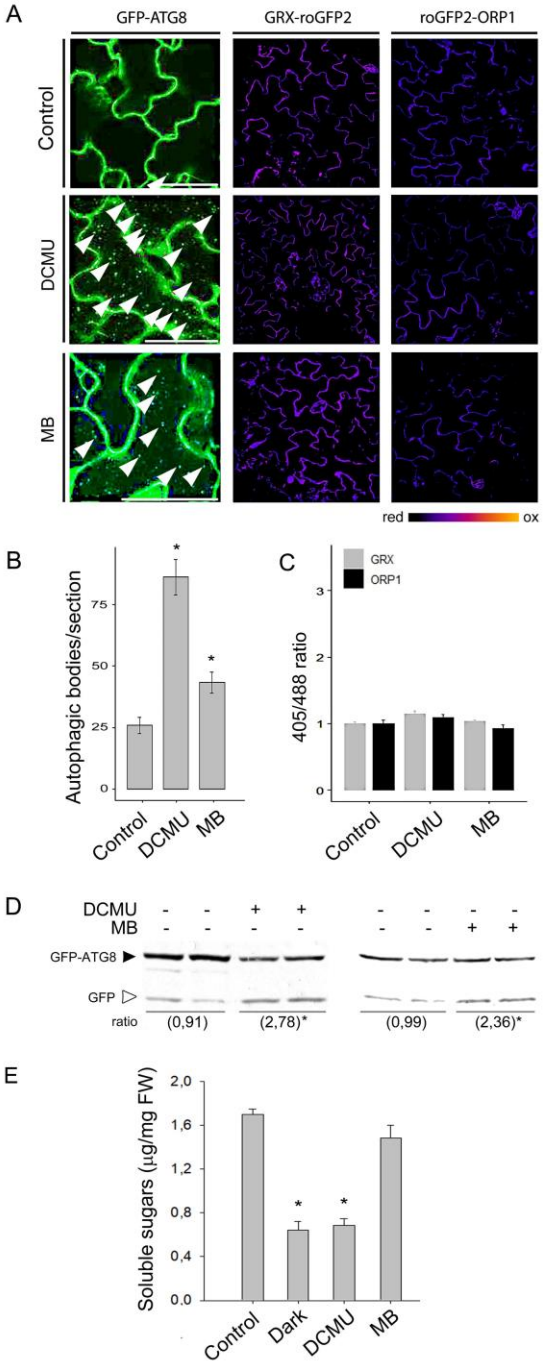

1004

1005

1006

1007

1008

1009

1010 **FIGURE 5**

1011

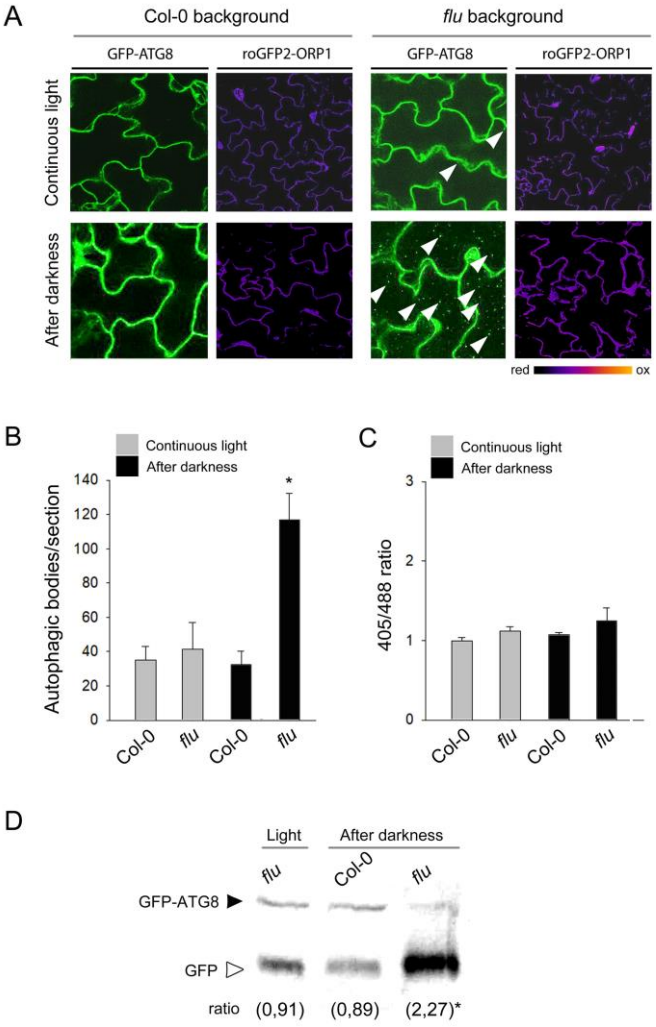

1012

1013

1014

1015